

**To cite this article:** HE H K, WANG N. Monocular visual servo-based stabilization control of underactuated unmanned surface vehicle[J/OL]. Chinese Journal of Ship Research, 2022, 17(5). <http://www.ship-research.com/en/article/doi/10.19693/j.issn.1673-3185.02853>.

**DOI:** 10.19693/j.issn.1673-3185.02853

# Monocular visual servo-based stabilization control of underactuated unmanned surface vehicle



HE Hongkun<sup>1</sup>, WANG Ning<sup>\*2</sup>

1 College of Marine Electrical Engineering, Dalian Maritime University, Dalian 116026, China

2 College of Marine Engineering, Dalian Maritime University, Dalian 116026, China

**Abstract:** [Objectives] Aiming at the accurate posture stabilization problem of an under-actuated unmanned surface vehicle (USV) in GPS-denied environments, a monocular visual servo stabilization control scheme is proposed based on homography. [Methods] By virtue of the homography decomposition technique, posture errors with an unknown scale factor are directly reconstructed from current and desired images, which thoroughly removes the calibration of extrinsic camera parameters and priori information on visual targets; with respect to the under-actuation constraint, a periodic function to persistently excite the yaw angle is incorporated into the continuous time-variant output feedback controller, allowing the USV to be stabilized in the absence of image depth, movement velocities and model parameters. [Results] Under the framework of the Lyapunov theory, the closed-loop visual servo system of the USV is rigorously proven to be asymptotically stable by Barbalat lemma. [Conclusions] By installing an onboard monocular camera, USV posture errors can be precisely stabilized with the aid of the proposed visual servo strategy, providing significant technique support for practical applications including docking, berthing, dynamic positioning, etc.

**Key words:** underactuated unmanned surface vehicle; monocular visual servo; stabilization control; continuous time-variant output feedbacks

**CLC number:** U664.82

## 0 Introduction

With the development of the economy and society, human activities on the water are increasingly frequent. Unmanned surface vehicles (USVs), as lightweight surface robots, can free human beings from repetitive and dangerous tasks, which have attracted extensive attention from researchers all over the world [1-4]. It is worth noting that motion control is the core technology to realize the autonomous operation of USVs, among which stabilization control is the basic problem of the USV motion control and has significant application value and market prospects in the fields of docking, berthing and unberthing,

ing, dynamic positioning, etc.

To reduce weight and cost, USVs are often equipped with two propellers or a single propeller and rudder at the stern, which can only provide surge thrust and yaw moment. In fact, this power allocation mode brings great difficulties to the design of the stabilization controller of USVs. The main reason is the underactuated property of USVs, which uses two control inputs to simultaneously stabilize the three motion states of the USVs, including the plane position and yaw angle. For the under-actuated stabilization system of USVs, due to the non-integrable second-order nonholonomic constraints, there is no continuous time-invariant feed-

**Received:** 2022 - 04 - 15

**Accepted:** 2022 - 08 - 11

**Supported by:** National Natural Science Foundation of China (52271306); Open Fund for Innovative Research on Ship Overall Performance (31422120)

**Authors:** HE Hongkun, male, born in 1988, doctoral candidate. Research interests: UAV visual servo control.

E-mail: [hehongkun4@163.com](mailto:hehongkun4@163.com)

WANG Ning, male, born in 1983, Ph.D., professor, doctoral supervisor. Research interests: intelligent control of ocean robots, unmanned ships, and autonomous systems. E-mail: [n.wang@ieee.org](mailto:n.wang@ieee.org)

**\*Corresponding author:** WANG Ning

back control law, which makes the system asymptotically stable in the sense of Lyapunov [5]. In addition, the underactuated USV stabilization system is highly nonlinear and cannot be converted into an integral chain form, making the standard chain system control method not directly applicable [6]. To solve the problem of stabilization control of underactuated USVs, global scholars have successively proposed the design methods of discontinuous time-invariant and continuous time-variant controllers. In the aspect of discontinuous time-invariant controller design, Reyhanoglu [7] proposed a  $\sigma$  transformation method to design discontinuous coordinate transformation on the premise that the yaw angle error was not zero and designed reduced order system control input in kinematics. Finally, a time-invariant discontinuous feedback control law was constructed to ensure that the posture error was asymptotically stable at an exponential convergence rate. Ghommam et al. [8] proposed the cascade control method, which used the differential homeomorphic coordinate transformation to transform the USV system into a cascade form. The original problem was simplified into the stabilization control problem of a third-order chained system. On the premise that the yaw angle error was not zero, the time-invariant discontinuous feedback control law was derived to ensure that the system was uniformly and asymptotically stable globally. In the aspect of continuous time-variant controller design, Pettersen et al. [9] put forward the homogeneous method, which represented the dynamics of the USV stabilization system in the body coordinate system by the coordinate transformation method, and they designed a time-variant feedback control law with periodic oscillation performance and proved the exponential convergence of the closed-loop system using the homogeneous degree and average theory. Mazenc et al. [10] proposed the backstepping design method, skillfully established the equivalent controlled system through coordinate transformation, and introduced the periodic function into the smooth time-variant state feedback controller so that the underactuated USV stabilization system was uniformly asymptotically stable globally in the sense of Lyapunov. Under the cascade control framework, Dong et al. [11] designed a global smooth time-variant control law using the backstepping method, making the closed-loop system state asymptotically converge to the origin. Dong et al. [12] put forward the block backstepping control method in the polar coordinate system, and

they transformed the underactuated USV stabilization control problem in the rectangular coordinate system into the fully driven stabilization control problem in the polar coordinate system by using the known sideslip angle, thus reducing the difficulty in controller design.

Although the research on the stabilization control of underactuated USVs has achieved fruitful theoretical results, most of the literature assumes that the position of USVs is precisely known. In fact, USVs often use GPS devices to measure the position and even movement velocity. Generally, the positioning accuracy is only on the level of meters [13]. In addition, in water areas such as ports and rivers sheltered by tall buildings or trees, GPS has the problem of signal attenuation and loss, which makes the above control algorithms unavailable in this scene. With the rapid development of artificial intelligence technology and computer computing ability, visual servo methods relying on the high-precision positioning ability of optical cameras show significant advantages in the motion control of USVs [14]. Compared with the binocular visual servo and multi-visual servo, the monocular visual servo processes fewer images, which can better meet the real-time computing requirements of the servo process. At present, the monocular visual servo is mainly used in docking and berthing tasks of USVs. In other countries, Martins et al. [15] assumed that the yellow underwater vehicle was floating on the water, and under the condition that the internal and external parameters of the monocular camera were calibrated, the relative position and direction between the USV and underwater vehicle were calculated. According to the distance between them, an event-triggered control strategy was designed, and the speed of the two propellers was controlled by proportional differential state feedback to complete the tasks of approach, alignment, and docking successively. Dunbabin et al. [16] used the calibrated height and inclination angle of the monocular camera to locate the position of the surface target. The virtual attractive and repulsive forces were generated according to the relative distance, and their resultant direction was set as the desired yaw angle of the USV. The proportional controller was used to adjust the output thrust of the two propellers and change the position and attitude of the USV, so as to realize the docking of the USV with the surface target. Kim et al. [17] used monocular vision to determine the position and attitude of the target when the

distance was relatively close. The proportional controller and modeless control strategy were designed using the pseudo-inverse technique and reinforcement learning method, respectively, to perform servo control on the docking between the USV and the surface robot. In China, Xu et al. [18] used the detection network to identify the suspended carrier, and the yaw angle of the USV was calculated according to its projected image and the internal parameters of the camera. Under the constant throttle, the rudder angle S-surface controller was designed by integrating the proportional differential signal of the deflection angle, and the USV kept approaching the carrier by controlling the rudder angle in real time until the docking task was completed. Zhang et al. [19] took the red rectangular surface as the identification marker of the monocular camera and used the current image, the desired image, the camera's internal parameters, and the marker's calibration height to calculate the course deviation angle and yaw distance of the USV, which were used as the control variables to design a proportional differential controller. It regulated the voltage of the two propulsion motors at the stern and changed the surge velocity and yaw angle rate of the USV, making the underactuated USV approach the berth along the marking line. Since it is an under-constrained problem to recover three-dimensional (3D) spatial information using two-dimensional (2D) images, the above monocular visual servo methods need to calibrate the external parameters of the camera or the model information of the known target in advance during relative positioning. To facilitate practical application, under the condition that the external parameters of the monocular camera were not calibrated, Wang et al. [20-22] adopted the servo strategy based on homography and researched the visual servo stabilization control of the fully driven USV. In Ref. [20], the posture error of the USV with a scale factor was directly obtained by the current and desired images. A monocular visual servo framework based on homography was established for the first time, and the unknown image depth was estimated by using the parameter adaptive method, which realized the asymptotic stability of the USV stabilization system. In Ref. [21], aiming at the problem of unknown image depth, model parameters of the USV, and external disturbance, a single hidden layer neural network was used to identify the unknown nonlinearity of the system, and an extreme learning-

based visual servo method was proposed. The controller and adaptive law were designed through the Lyapunov function to make the posture error of the fully driven USV uniformly bounded. Considering that it was difficult to measure the movement velocity of the USV in the GPS-denied environment, Ref. [22] recovered the system state through a finite time observer and formed a visual servo strategy with output feedback. The asymptotic stability of the fully driven USV stabilization system was achieved by using only an onboard monocular camera.

Inspired by the above literature, this paper will research the monocular visual servo-based stabilization control of the underactuated USV, which relies only on one eye to achieve the underactuated USV gradually approaching the desired posture. Firstly, the homography decomposition technique is used to directly reconstruct the posture error of the USV from the current and desired images without calibrating the external parameters of the camera or the model information of the known target in advance. Different from the control system using GPS, the homography decomposition technique will inevitably lead to the unknown image depth appearing in the USV kinematics subsystem and make the coordinate transformation method [7-11], which avoids the underactuated constraints, no longer applicable. Secondly, considering the practical problem that the movement velocity and model parameters of the USV are difficult to obtain accurately, a continuous time-variant output feedback controller is designed to overcome the non-integrable second-order non-holonomic constraints, and it does not depend on the velocity state and model parameters. Then, under the framework of the Lyapunov theory, the stability of the closed-loop servo control system is rigorously proved by the Barbalat lemma. Finally, the simulation experiment verifies the effectiveness of the visual servo strategy. The proposed monocular visual servo control scheme can realize the asymptotic stability of the underactuated USV stabilization control system under the condition that the image depth, movement velocity, and model parameters are unknown. This research work can expand the application of the underactuated USV in a GPS-denied environment, enrich the stabilization control theory of the underactuated USV, and improve the autonomy and intelligence of the underactuated USV.

# 1 Basic knowledge and problem description

## 1.1 Basic knowledge

For the convenience of reading, the key lemmas involved in this paper, such as the matrix positive definite discriminant method, Hurwitz criterion, and Barbalat lemma, are stated as follows.

**Lemma 1** <sup>[23]</sup>: Let matrix  $A \in \mathbf{R}^{n \times n}$  and  $A = A^T$ , where  $\mathbf{R}$  represents the set of real numbers. If each order principal minor determinant of  $A$ , i.e.  $\Delta_i > 0$  ( $i = 1, \dots, n$ ), then  $A$  is positive definite.

**Lemma 2** <sup>[24]</sup>: Let the characteristic polynomial of the second-order linear time-invariant system, i.e.  $\dot{x} = Ax$ , be  $a_2s^2 + a_1s + a_0 = 0$ . If  $a_i > 0$  ( $i = 0, 1, 2$ ), then there is a positive definite matrix  $P \in \mathbf{R}^{2 \times 2}$ , which makes the Lyapunov equation  $A^T P + PA = -I$  have a unique solution, where  $I \in \mathbf{R}^{2 \times 2}$  is an identity matrix.

**Lemma 3** <sup>[25]</sup>: Make the function  $\varphi: [0, \infty) \rightarrow \mathbf{R}$  be square-integrable, that is  $\lim_{t \rightarrow \infty} \int_0^t \varphi^2(s) ds < \infty$ . If  $\dot{\varphi}(t)$  exists and is bounded, then  $\lim_{t \rightarrow \infty} \varphi(t) = 0$ .

**Lemma 4** <sup>[26]</sup>: When the function  $\varphi: [0, \infty) \rightarrow \mathbf{R}$  is uniformly continuous, if  $\lim_{t \rightarrow \infty} \int_0^t \varphi(s) ds$  exists and is bounded, then  $\lim_{t \rightarrow \infty} \varphi(t) = 0$ .

## 1.2 Model of USV stabilization control system

The maneuvering tasks such as berthing and unberthing, docking, and dynamic positioning completed by the under-actuated USV on the water surface can be abstracted as the stabilization control problem from the current posture to the desired posture, and its mathematical model of kinematics and dynamics can be described as <sup>[6-11]</sup>

$$\begin{cases} \dot{\eta} = R(\psi)v \\ M\dot{v} = -C(v)v - D(v)v + \tau \end{cases} \quad (1)$$

where

$$C(v) = \begin{bmatrix} 0 & 0 & -m_{22}v \\ 0 & 0 & m_{11}u \\ m_{22}v & -m_{11}u & 0 \end{bmatrix}$$

$$R(*) = \begin{bmatrix} \cos(*) & -\sin(*) & 0 \\ \sin(*) & \cos(*) & 0 \\ 0 & 0 & 1 \end{bmatrix}$$

where  $\eta = [x, y, \psi]^T$  is the current posture vector, including the position  $(x, y)$  and yaw angle  $\psi$  of the USV in the inertial coordinate system. The units of the position variable and the attitude variable are m

and rad, respectively;  $v = [u, v, r]^T$  is the velocity vector, which represents the surge/sway velocity  $(u, v)$  and the yaw angle rate  $r$  of the USV in the body coordinate system. The units of the linear velocity and the angular velocity are m/s and rad/s, respectively;  $\tau = [\tau_u, 0, \tau_r]^T$  is the system control input vector, and the units of the input force and the input torque are N and N·m, respectively;  $M = \text{diag}(m_{11}, m_{22}, m_{33}) > 0$  and  $D(v) = \text{diag}(d_{11}, d_{22}, d_{33}) > 0$  are the inertia mass matrix and system damping matrix, respectively;  $C(v)$  is the Coriolis centripetal force matrix;  $R(*)$  is the rotation matrix function of the attitude variable  $*$ .

To adjust the USV from the current posture to the desired posture, the posture error vector is defined as  $e = R^T(\psi)(\eta_d - \eta)$ . Combined with Eq. (1), by the derivation of  $e$ , the stabilization error dynamics can be obtained as follows.

$$\begin{cases} \dot{e}_1 = -u + e_2 r \\ \dot{e}_2 = -v - e_1 r \\ \dot{e}_3 = -r \end{cases} \quad (2)$$

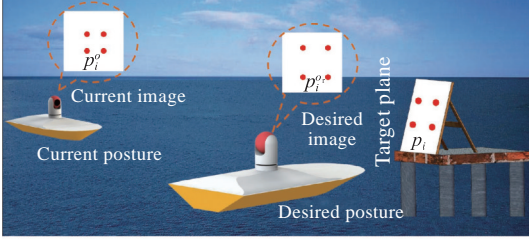
where  $e := [e_1, e_2, e_3]^T$ ;  $\eta_d = [x_d, y_d, \psi_d]^T$  is the constant desired posture vector.

## 1.3 Monocular visual servo dynamics of USV

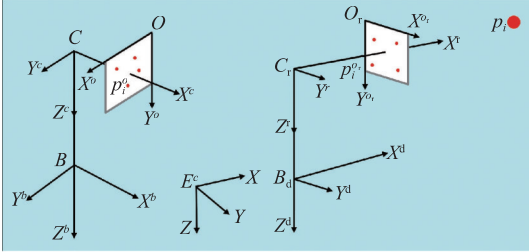
The current position  $(x, y)$  and the desired position  $(x_d, y_d)$  of the USV are difficult to obtain in a GPS-denied environment. To this end, a monocular camera was installed on the USV, as shown in Fig. 1(a), to sense the surrounding environment and achieve relative positioning. In addition, a series of feature points (red light emitting diode (LED) in Fig. 1(a)) were arranged on the target plane to form a monocular visual servo-based stabilization control task scene of USVs based on homography.

To facilitate the following description of the meaning of each parameter, 3D coordinate systems corresponding to Fig. 1 (a) were established according to the right-hand rule, as shown in Fig. 1(b), including the earth inertial coordinate system  $E\text{-}XYZ$ , the USV body coordinate system  $B\text{-}X^b Y^b Z^b$ , and the camera coordinate system  $C\text{-}X^c Y^c Z^c$ . The origin  $C$  is the optical center of the camera, and the optical axis  $X^c$  is oriented straight ahead of the bow;  $B\text{-}X^b Y^b Z^b$  is located below  $C\text{-}X^c Y^c Z^c$  and keeps a fixed parallel relationship with it;  $E\text{-}XYZ$  is the lower north east coordinate system as usual. In addition,  $O\text{-}X^o Y^o$  is a 2D image coordinate system, where the origin  $O$  is located in the top left corner of the image, the  $X^o$  axis is horizontally pointing to the right, and the  $Y^o$  axis

is vertically pointing to the bottom. Correspondingly,  $B_d - X^d Y^d Z^d$ ,  $C_r - X^c Y^c Z^c$ , and  $O_r - X^o Y^o Z^o$  are the USV, camera, and image coordinate systems under the desired posture.



(a) USV monocular camera, images, and feature points



(b) Inertial, body, camera, and image coordinate systems

Fig. 1 The monocular visual-servo system of underactuated USV

In  $E$ - $XYZ$ , the 3D coordinates of feature points are expressed by  $\mathbf{p}_i$ , where the subscript  $i$  represents the  $i$ -th feature point. As a reference signal, the desired image containing feature points is captured by a monocular camera in advance in  $C_r - X^c Y^c Z^c$ . Correspondingly, the actual signal is represented by the current image and can be acquired in real-time in  $C - X^c Y^c Z^c$ . According to the camera pinhole imaging model<sup>[20]</sup>, there is

$$\mathbf{p}_i^o = \frac{1}{x_i^c} \mathbf{T}_c \mathbf{p}_i^c, \quad \mathbf{p}_i^{o_r} = \frac{1}{x_i^{c_r}} \mathbf{T}_c \mathbf{p}_i^{c_r} \quad (3)$$

where

$$\mathbf{T}_c = \begin{bmatrix} x_c^o & a_x & 0 \\ y_c^o & 0 & a_y \\ 1 & 0 & 0 \end{bmatrix}$$

Specifically,  $\mathbf{p}_i^o = [x_i^o, y_i^o, 1]^T$  and  $\mathbf{p}_i^{o_r} = [x_i^{o_r}, y_i^{o_r}, 1]^T$  respectively represent the homogeneous projection coordinates of  $\mathbf{p}_i$  in  $O - X^o Y^o Z^o$  and  $O_r - X^{o_r} Y^{o_r} Z^{o_r}$  coordinate systems, with the unit being the pixel, which can be obtained through target recognition algorithms<sup>[27]</sup>;  $\mathbf{p}_i^c = [x_i^c, y_i^c, z_i^c]^T$  and  $\mathbf{p}_i^{c_r} = [x_i^{c_r}, y_i^{c_r}, z_i^{c_r}]^T$  are respectively the position coordinates of  $\mathbf{p}_i$  in  $C - X^c Y^c Z^c$  and  $C_r - X^{c_r} Y^{c_r} Z^{c_r}$  coordinate systems;  $\mathbf{T}_c$  is the calibrated camera internal parameter matrix<sup>[28]</sup>;  $(x_c^o, y_c^o)$  is the coordinate of the principal point of the image;  $a_x$  and  $a_y$  are the focal lengths in the corresponding direction.

Actually,  $\mathbf{p}_i^o$  and  $\mathbf{p}_i^{o_r}$  have the following coordinate transformation relations with  $\mathbf{p}_i$ , respectively.

$$\mathbf{p}_i^c = \mathbf{R}^T(\psi)(\mathbf{p}_i - \mathbf{p}_c), \quad \mathbf{p}_i^{c_r} = \mathbf{R}^T(\psi_r)(\mathbf{p}_i - \mathbf{p}_{c_r}) \quad (4)$$

where  $\mathbf{p}_c = [x, y, -h_c]^T$  and  $\mathbf{p}_{c_r} = [x_r, y_r, -h_{c_r}]^T$  are respectively the position coordinates of the optical centers  $C$  and  $C_r$  in the coordinate system  $E$ - $XYZ$ ;  $h_c$  is the camera height. In addition, according to the epipolar geometry principle<sup>[21]</sup>,  $\mathbf{p}_i^o$  and  $\mathbf{p}_i^{o_r}$  have the following projection relationship.

$$\mathbf{p}_i^o = \mathbf{T}_c \mathbf{H} \mathbf{T}_c^{-1} \mathbf{p}_i^{o_r} \quad (5)$$

where  $\mathbf{H} \in \mathbf{R}^{3 \times 3}$  is the Euclidean homography matrix. When  $i \geq 3$ ,  $\mathbf{H}$  can be obtained by solving Eq. (5)<sup>[29]</sup>.

Combining Eqs. (3) - (5), we can get

$$\mathbf{p}_i - \mathbf{p}_c = \frac{x_i^c}{x_i^{c_r}} \mathbf{R}(\psi) \mathbf{H} \mathbf{R}^T(\psi_r) (\mathbf{p}_i - \mathbf{p}_{c_r}) \quad (6)$$

Therefore, the homography matrix  $\mathbf{H}$  can be expressed as

$$\mathbf{H} = \frac{x_i^{c_r}}{x_i^c} (\mathbf{R}(e_3) + \frac{\mathbf{t}_{c_r}^c}{d} \mathbf{n}_r^T) \quad (7)$$

where  $\mathbf{t}_{c_r}^c = \mathbf{R}^T(\psi)(\mathbf{p}_{c_r} - \mathbf{p}_c)$  is the camera translation vector  $[e_1, e_2, 0]^T$ ;  $d = \mathbf{n}_r^T \mathbf{R}^T(\psi_r)(\mathbf{p}_i - \mathbf{p}_{c_r}) > 0$ , is the vertical distance from  $C_r$  to the target plane, namely, the inherent unknown image depth;  $\mathbf{n}_r \in \mathbf{R}^3$  is the unit normal vector of the target plane in the coordinate system  $C_r - X^{c_r} Y^{c_r} Z^{c_r}$ .

Obviously, the homography matrix  $\mathbf{H}$  implies the stabilization control error information  $\mathbf{e}$  of the USV. By using the homography decomposition technique<sup>[30]</sup> to decompose the matrix  $\mathbf{H}$ , the translation error  $(e_x, e_y)$  and rotation error  $e_\psi$  with a scale factor can be directly obtained, namely,

$$e_x = \frac{e_1}{d}, \quad e_y = \frac{e_2}{d}, \quad e_\psi = e_3 \quad (8)$$

Therefore, by taking the derivation of Eq. (1), Eq. (2), and Eq. (8) with respect to the available errors  $e_x$ ,  $e_y$ , and  $e_\psi$ , the monocular visual servo-based stabilization control system of the underactuated USV can be obtained as shown in Eq. (9).

$$\begin{cases} d\dot{e}_x = -u + de_y r \\ d\dot{e}_y = -v - de_x r \\ \dot{e}_\psi = -r \\ m_{11}\dot{u} = m_{22}vr - d_{11}u + \tau_u \\ m_{22}\dot{v} = -m_{11}ur - d_{22}v \\ m_{33}\dot{r} = (m_{11} - m_{22})uv - d_{33}r + \tau_r \end{cases} \quad (9)$$

In order to realize the monocular visual servo-based stabilization control of USVs, the following assumptions are made in this paper.

**Assumption 1:** The USV is equipped with one sensor, that is, a wide-angle monocular camera, which can keep the feature points in the field of view all the time, so the image depth  $d$  and movement velocity  $(u, v, r)$  are unknown.

**Assumption 2:** The motion characteristics of the

USV can be expressed by the classical mathematical model of Eq. (1). In other words, the internal unmodeled dynamics and external disturbances can be ignored, and the dynamic model parameters, namely,  $(m_{11}, m_{22}, m_{33})$  and  $(d_{11}, d_{22}, d_{33})$ , of the USV are unidentified.

**Control target:** When assumption 1 and assumption 2 are satisfied, only a monocular camera is used to measure information  $(e_x, e_y, e_\psi)$  and design the control law of  $\tau_u$  and  $\tau_r$  for the USV motion system of Eq. (1), which makes the posture error  $(e_1, e_2, e_3)$  and movement velocity  $(u, v, r)$  of the USV asymptotically stable, so as to realize the stabilization control of the underactuated USV, namely,  $\eta \rightarrow \eta_d$  when  $t \rightarrow \infty$ .

It is noted that although the laser rangefinder, doppler log, and inertial navigation unit can directly measure the image depth  $d$  and the movement velocity  $(u, v, r)$  of the USV, carrying more sensors will inevitably increase the energy consumption and manufacturing costs of USVs. In addition, semi-empirical methods, software packages, and physical experiments can be used to identify the inertial parameters  $(m_{11}, m_{22}, m_{33})$  of USVs [31], but this way will cost a lot of manpower and material resources, and the damping parameters  $(d_{11}, d_{22}, d_{33})$  are actually very difficult or impossible to be accurately identified [32]. Therefore, for the practical problems of the monocular visual servo-based stabilization control of underactuated USVs, this paper gives reasonable assumption 1 and assumption 2. Obviously, un-

der the premise that the image depth, movement velocity, and model parameters are unknown, the USV monocular visual servo system of Eq. (9) has unknown kinematics and dynamics, which leads to the inapplicability of the coordinate transformation method [7-11] to solve the underactuated problem. It can be seen that it is of practical significance and serves as a theoretical challenge to design a stable underactuated USV dynamics controller to asymptotically stabilize the posture errors by using only monocular vision measurement information.

## 2 Controller design and stability analysis

### 2.1 Controller design

In addition to closed-loop control, image processing, target identification, image matching, homography matrix calculation and decomposition, and other operations are also inevitably involved in the USV monocular visual servo system, which requires a large amount of computation. To ensure the real-time performance of the entire visual servo system, this paper does not use the parameter adaptive method [20] to estimate the image depth online, nor does it design an observer [22] to reconstruct the movement velocity of the USV, which can reduce the complexity of the controller and the computational consumption. Fig. 2 is the block diagram of the monocular visual-servo stabilization control system.

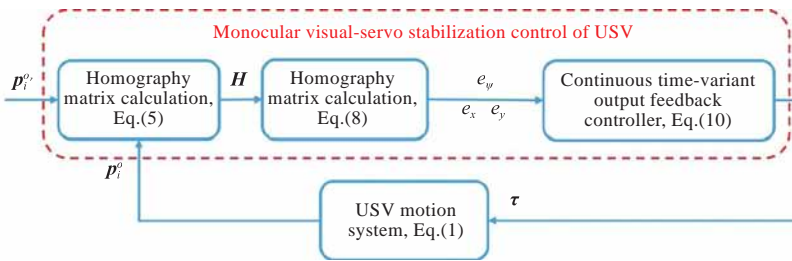


Fig. 2 The block diagram of monocular visual-servo stabilization control system

In the USV monocular visual-servo stabilization control system, the projection points  $P_i^o$  and  $P_i^c$  in the desired and current images are first used to calculate the matrix  $H$ , and the homography decomposition technique is then used to decompose the matrix to directly obtain the visual servo stabilization error  $(e_x, e_y, e_\psi)$ . Finally, under the premise that the image depth, movement velocity, and model parameters are unknown, in order to make the underactuated USV monocular visual servo system of Eq. (9) asymptotically stable, the continuous time-variant

output feedback controller is designed as

$$\begin{cases} \tau_u = k_1 e_x \\ \tau_r = k_2 e_\psi + k_3 e_y \sin(k_4 t) \end{cases} \quad (10)$$

where  $0 < k_1 < \frac{dd_{11}d_{22}}{m_{11}}$ ,  $k_2 > 0$ ,  $k_3 > 0$ , and  $k_4 \neq 0$  are all design adjustment parameters.

It can be seen from Eq. (10) that the output feedback controller designed in this paper has only four adjustment parameters, each of which has physical significance and is convenient for adjusting the control performance. Intuitively,  $k_1$  is the feedback

gain, which determines the control input  $\tau_u$  and is used to adjust the convergence rate of the longitudinal error  $e_x$ ;  $\tau_r$  is coupled by the attitude error  $e_\psi$  and the transverse error  $e_y$ ;  $k_2$  and  $k_3$  are feedback gains. When the longitudinal error  $e_y$  is not zero, the time-variant sine function will generate a continuous excitation signal, and  $k_4$  is used to adjust the period of the excitation signal, so as to change the yaw angle of the USV, eliminate the longitudinal error  $e_y$ , and solve the underactuated problem of the USV. When the longitudinal error  $e_y$  is 0,  $\tau_r$  only feedbacks the attitude error  $e_\psi$ , and the yaw angle of the USV is finally stabilized to the desired direction.

## 2.2 Stability analysis

**Theorem 1:** Considering the underactuated USV monocular visual servo system of Eq. (9), we select the control design parameters, which satisfy  $0 < k_1 < \frac{dd_{11}d_{22}}{m_{11}}$ ,  $k_2 > 0$ ,  $k_3 > 0$ , and  $k_4 \neq 0$ . The proposed continuous time-variant output feedback controller of Eq. (10) proposed in this paper can asymptotically stabilize the posture error ( $e_1$ ,  $e_2$ ,  $e_3$ ) and movement velocity ( $u$ ,  $v$ ,  $r$ ) of the USV using only the onboard monocular camera to measure information ( $e_x$ ,  $e_y$ ,  $e_\psi$ ) when the image depth, the velocity of the USV, and the model parameters are unknown.

**Proof:** The system state ( $e_1$ ,  $u$ ,  $e_2$ ,  $v$ ) is uniformly bounded; the system state ( $e_3$ ,  $r$ ) is uniformly bounded; the system state ( $e_1$ ,  $u$ ,  $e_2$ ,  $v$ ,  $e_3$ ,  $r$ ) is asymptotically stable.

We substitute the control input of Eq. (10) into the USV monocular visual servo system of Eq. (9) to obtain a closed-loop control system.

$$\dot{e}_x = -\frac{u}{d} + e_y r \quad (11)$$

$$\dot{u} = \frac{k_1 e_x}{m_{11}} - \frac{d_{11} u}{m_{11}} + \frac{m_{22} v r}{m_{11}} \quad (12)$$

$$\dot{e}_y = -\frac{v}{d} - e_x r \quad (13)$$

$$\dot{v} = -\frac{d_{22} v}{m_{22}} - \frac{m_{11} u r}{m_{22}} \quad (14)$$

$$\dot{e}_\psi = -r \quad (15)$$

$$\dot{r} = \frac{k_2 e_\psi}{m_{33}} - \frac{d_{33} r}{m_{33}} + \frac{(m_{11} - m_{22}) u v}{m_{33}} + \frac{k_3 e_y \sin(k_4 t)}{m_{33}} \quad (16)$$

1) The system state ( $e_1$ ,  $u$ ,  $e_2$ ,  $v$ ) is uniformly bounded. We select two symmetric matrices, namely,

$$\mathbf{P}_1 = \begin{bmatrix} d & -\frac{m_{11}}{d_{22}} \\ -\frac{m_{11}}{d_{22}} & \frac{m_{11}(d_{11} + d_{22})}{k_1 d_{22}} \end{bmatrix} \quad (17)$$

$$\mathbf{P}_2 = \begin{bmatrix} d & -\frac{m_{22}}{d_{22}} \\ -\frac{m_{22}}{d_{22}} & \frac{m_{22}^2(d_{11} + d_{22})}{k_1 m_{11} d_{22}} \end{bmatrix} \quad (18)$$

where  $d > 0$ . The determinants of them are as follows.

$$|\mathbf{P}_1| = \frac{m_{11}(dd_{11}d_{22} - m_{11}k_1 + dd_{22}^2)}{k_1 d_{22}^2} > 0 \quad (19)$$

$$|\mathbf{P}_2| = \frac{m_{22}^2(dd_{11}d_{22} - m_{11}k_1 + dd_{22}^2)}{k_1 m_{11} d_{22}^2} > 0 \quad (20)$$

According to lemma 1,  $\mathbf{P}_1$  and  $\mathbf{P}_2$  are positive definite matrices. Using the positive definiteness of  $\mathbf{P}_1$  and  $\mathbf{P}_2$ , the Lyapunov function is constructed as follows.

$$V_1 = \mathbf{x}_1^T \mathbf{P}_1 \mathbf{x}_1 + \mathbf{x}_2^T \mathbf{P}_2 \mathbf{x}_2 \quad (21)$$

where  $\mathbf{x}_1 = [e_x, u]^T$ ;  $\mathbf{x}_2 = [e_y, v]^T$ .

Taking the derivation of Eqs. (11)-(14) with respect to  $V_1$ , we can get

$$\dot{V}_1 = -\frac{1}{d_{22}} \mathbf{x}_1^T \mathbf{Q} \mathbf{x}_1 - av^2 \quad (22)$$

where

$$a = \frac{m_{22}(dd_{11}d_{22} - m_{11}k_1 + dd_{22}^2)}{k_1 m_{11} dd_{22}} > 0$$

$$\mathbf{Q} = \begin{bmatrix} k_1 & -d_{11} \\ -d_{11} & \frac{dd_{11}d_{22} - m_{11}k_1 + dd_{22}^2}{k_1 d} \end{bmatrix}$$

Since  $k_1 > 0$  and  $|\mathbf{Q}| = \frac{dd_{11}d_{22} - m_{11}k_1}{d} > 0$ , so  $\mathbf{Q}$  is a positive definite matrix according to lemma 1. According to Eq. (22),  $\dot{V}_1 \leq 0$ , namely,  $V_1(t) \leq V_1(0)$ . When the initial value  $V_1(0)$  is bounded, and the system state ( $e_x$ ,  $u$ ,  $e_y$ ,  $v$ ) is uniformly bounded, namely,  $e_x \in L_\infty$ ,  $u \in L_\infty$ ,  $e_y \in L_\infty$ , and  $v \in L_\infty$ . It can be seen from Eq. (8) that the system state ( $e_1$ ,  $e_2$ ) is also uniformly bounded.

2) The system state ( $e_3$ ,  $r$ ) is uniformly bounded. Eqs. (15)~(16) of the system are rewritten into the following vector form.

$$\dot{\mathbf{x}}_3 = \mathbf{A} \mathbf{x}_3 + \mathbf{b} \quad (23)$$

where

$$\mathbf{x}_3 = [e_\psi, r]^T$$

$$\mathbf{A} = \begin{bmatrix} 0 & -1 \\ \frac{k_2}{m_{33}} & -\frac{d_{33}}{m_{33}} \end{bmatrix}$$

$$\mathbf{b} = \left[ 0, \frac{(m_{11} - m_{22})uv}{m_{33}} + \frac{k_3 e_y \sin(k_4 t)}{m_{33}} \right]^T$$

where  $\mathbf{x}_3$  represents the system state vector;  $\mathbf{A}$  is the gain matrix;  $\mathbf{b}$  can be regarded as time-variant disturbances. The characteristic polynomial of the linear time-invariant system  $\dot{\mathbf{x}}_3 = \mathbf{A} \mathbf{x}_3$  is  $m_{33}s^2 + d_{33}s + k_2 = 0$ . According to lemma 2, there is a unique positive definite matrix  $\mathbf{P}_3 \in \mathbf{R}^{2 \times 2}$  that satisfies  $\mathbf{A}^T \mathbf{P}_3 +$

$$P_3A = -I.$$

The Lyapunov function is constructed as follows.

$$V_2 = \mathbf{x}_3^T P_3 \mathbf{x}_3 \tag{24}$$

Taking the derivation of Eq. (23) with respect to  $V_2$ , we can get

$$\dot{V}_2 = -\mathbf{x}_3^T (A^T P_3 + P_3 A) \mathbf{x}_3 + \mathbf{x}_3^T \delta = -\mathbf{x}_3^T \mathbf{x}_3 + \mathbf{x}_3^T \delta \tag{25}$$

where  $\delta = 2P_3 \mathbf{b}$ . It can be seen from Eq. (22) and Eq. (23) that the system state  $(e_y, u, v)$  is bounded, so there is an upper bound value  $\bar{\delta} > 0$ , and it satisfies  $\|\delta\| \leq \bar{\delta}$ .

By using Young's inequality of Eq. (26), Eq. (25) is rewritten into the form of Eq. (27).

$$\mathbf{x}_3^T \delta \leq \theta \|\mathbf{x}_3\|^2 + \frac{\bar{\delta}^2}{4\theta} \tag{26}$$

$$\dot{V}_2 \leq -(1-\theta)\|\mathbf{x}_3\|^2 + \frac{\bar{\delta}^2}{4\theta} \leq -\frac{1-\theta}{\lambda_{\max}(P_3)} V_2 + \frac{\bar{\delta}^2}{4\theta} \tag{27}$$

where  $\theta \in (0, 1)$ ;  $\lambda_{\max}(P_3) > 0$  is the largest eigenvalue of the positive definite matrix  $P_3$ . The inequality of Eq. (27) shows that when

$$V_2 > \frac{\lambda_{\max}(P_3)\bar{\delta}^2}{4\theta(1-\theta)}, \quad \dot{V}_2 < 0$$

the system state  $(e_y, r)$  converges to the set

$$\Omega = \left\{ V_2 \left| V_2 \leq \frac{\lambda_{\max}(P_3)\bar{\delta}^2}{4\theta(1-\theta)} \right. \right\}$$

and then we have  $e_y \in \mathcal{L}_\infty$  and  $r \in \mathcal{L}_\infty$ . It can be seen from  $e_3 = e_y$  that  $e_3$  is uniformly bounded.

3) The system state  $(e_1, u, e_2, v, e_3, r)$  is asymptotically stable. Since the system state  $(e_x, e_y, e_\psi, u, v, r)$  is uniformly bounded, its derivative  $(\dot{e}_x, \dot{e}_y, \dot{e}_\psi, \dot{u}, \dot{v}, \dot{r})$  is also uniformly bounded according to Eqs. (11)-(16).

It can be obtained from Eq. (22) that

$$\int_0^\infty v^2(s)ds \leq -\frac{1}{a} \int_0^\infty \dot{V}_1(s)ds = \frac{1}{a} (V_1(0) - V_1(\infty)) \tag{28}$$

so  $v \in \mathcal{L}_2$  and  $\dot{v} \in \mathcal{L}_\infty \Rightarrow v$  is uniformly continuous. According to lemma 3,  $\lim_{t \rightarrow \infty} v(t) = 0$ . Similarly, it is easy to prove  $\lim_{t \rightarrow \infty} e_x(t) = 0$  and  $\lim_{t \rightarrow \infty} u(t) = 0$  according to Eq. (22).

By combining the uniform continuity of  $e_\psi \in \mathcal{L}_\infty$  and  $\ddot{e}_\psi = -\dot{r} \in \mathcal{L}_\infty \Rightarrow \dot{e}_\psi = -r$  and referring to lemma 4, there is  $\lim_{t \rightarrow \infty} r(t) = 0$ .

Besides, since  $\tau_r = k_2 e_\psi + k_3 e_y \sin(k_4 t) \in \mathcal{L}_\infty$  and

$$\begin{aligned} \ddot{\tau}_r = & -k_2 \dot{r} - \frac{k_3}{d} \dot{v} \sin(k_4 t) - \frac{k_3 k_4}{d} v \cos(k_4 t) - \\ & k_3 \dot{e}_x r \sin(k_4 t) - k_3 e_x \dot{r} \sin(k_4 t) - k_3 k_4 e_x r \cos(k_4 t) + \\ & k_3 k_4 \dot{e}_y \cos(k_4 t) - k_3 k_4^2 \sin(k_4 t) \end{aligned} \tag{29}$$

$\ddot{\tau}_r \in \mathcal{L}_\infty \Rightarrow \dot{\tau}_r$  is uniformly continuous. According to lemma 4, we have  $\lim_{t \rightarrow \infty} \dot{\tau}_r(t) = 0$ . By using  $\lim_{t \rightarrow \infty} r(t) = 0$ ,  $\lim_{t \rightarrow \infty} e_x(t) = 0$ , and

$$\dot{\tau}_r = -k_2 r - \frac{k_3}{d} v \sin(k_4 t) - k_3 e_x r \sin(k_4 t) + k_3 k_4 e_y \cos(k_4 t) \tag{30}$$

we can directly get  $\lim_{t \rightarrow \infty} e_y(t) = 0$ . Because  $r \in \mathcal{L}_\infty$  and  $\ddot{r} = -\frac{d_{33}\dot{r}}{m_{33}} + \frac{(m_{11}-m_{22})\dot{u}v}{m_{33}} + \frac{(m_{11}-m_{22})u\dot{v}}{m_{33}} + \dot{\tau}_r$ , (31)

$\ddot{r} \in \mathcal{L}_\infty \Rightarrow \dot{r}$  is uniformly continuous. According to lemma 4, it can be proved that  $\lim_{t \rightarrow \infty} \dot{r}(t) = 0$ . Since  $\lim_{t \rightarrow \infty} r(t) = 0$ ,  $\lim_{t \rightarrow \infty} u(t) = 0$ ,  $\lim_{t \rightarrow \infty} v(t) = 0$ , and  $\lim_{t \rightarrow \infty} e_y(t) = 0$ , we can finally prove that  $\lim_{t \rightarrow \infty} e_\psi(t) = 0$  according to Eq. (16).

In summary, the system state  $(e_x, u, e_y, v, e_\psi, r)$  is asymptotically stable. According to Eq. (8), the asymptotic stability of  $(e_1, e_2, e_3)$  can be directly proved. Theorem 1 is thus proved.

### 3 Simulation experiments

In this paper, simulation experiments were carried out by taking the famous Cybership I underactuated USV as the model to verify the effectiveness of the continuous time-variant output feedback controller of Eq. (10). The USV was developed by the Norwegian University of Science and Technology based on a large supply ship, with a scale ratio of 1:70, a length of 1.19 m, and a weight of 17.6 kg. Its main model parameters are shown in Table 1.

Table 1 Model parameters of the Cybership I<sup>[33]</sup>

Parameter	Value	Parameter	Value
$m_{11}$	19	$d_{11}$	4
$m_{22}$	35.2	$d_{22}$	1
$m_{33}$	4.2	$d_{33}$	10

In order to establish the USV monocular visual servo simulation scene, four feature points are arranged on the target plane, whose 3D spatial positions are  $\mathbf{p}_1 = [0.8, -, -0.2]^T$ ,  $\mathbf{p}_2 = [0.8, 1, -0.2]^T$ ,  $\mathbf{p}_3 = [0.8, 1, -2.2]^T$ , and  $\mathbf{p}_4 = [0.8, -1, -2.2]^T$ , respectively. The camera height is set to  $h_c = 1$ . The USV obtains the desired image in advance at the posture of  $\boldsymbol{\eta}_d = [0, 0, 0]^T$ , so the image depth is  $d = 0.8$ . In order to enable the monocular camera to capture feature points at the initial moment, the initial state of the USV is set as  $\boldsymbol{\eta}(0) = [-10, -10, 1.5]^T$  and  $\mathbf{v}(0) = [0, 0, 0]^T$ . In other words, the USV is in a static state. It should be noted that for the USV controller, the 3D spatial position of the above feature points, camera height, UAV model parameters, desired posture, and initial state are all unknown. In the monocular visual servo-based stabilization control of USVs, firstly, the initial and desired images are generated by using Eq. (3), and the projection coordinates  $\mathbf{p}_i^o(0)$  and  $\mathbf{p}_i^c$  of the feature points can be determined by the recognition algorithm. Then, the

calibrated camera internal parameters  $x_c = y_c = 512$  and  $a_x = a_y = 200$  are used to solve Eq. (5), so as to obtain the homography matrix  $H$ . Finally, the matrix is decomposed by the homography decomposition technique and the visual servo initial errors, namely,  $e_x(0) = 13.35$ ,  $e_y(0) = -11.58$ , and  $e_\psi(0) = -1.5$ , are obtained. It can be seen from theorem 1 that the gain parameters of the controller of Eq. (10) must meet the following conditions, namely,  $0 < k_1 < \frac{dd_{11}d_{22}}{m_{11}}$ ,  $k_2 > 0$ ,  $k_3 > 0$ , and  $k_4 \neq 0$ . The maximum input force and torque of the Cybership I are about 2 N and 1.5 N·m, respectively.

In conclusion, the gain parameters are conservatively set to a smaller value, that is,  $k_1 = k_2 = k_3 = 0.06$ , so as to meet the selection requirements of gain parameters and avoid control input saturation. In addition, in order to avoid over-frequency excitation, the excitation period is about 30 s, and  $k_4 = 0.2$  is set. In the simulation experiments, the wide-angle camera is selected to lower the risk of feature targets going out of view, and the image resolution is selected as  $1024 \times 1024$ .

The simulation results are shown in Figs. 3–7. In order to save space, the desired and current images at each moment are drawn in the same image to form the motion trajectory of feature points in the image space. With the motion of the USV, the current image tends to overlap with the desired image, as shown in Fig. 3. In the visual servo process, the Euclid homography matrix is calculated by using the current and desired images, and the posture errors related to the unknown image depth are obtained by decomposing the matrix, as shown in Fig. 4. Therefore, it is not necessary to calibrate the external parameters of the camera or know the target model information in advance, which facilitates

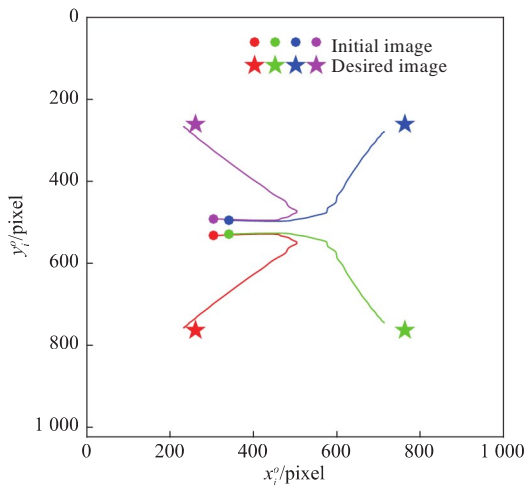


Fig. 3 The trajectories of feature points in the image space

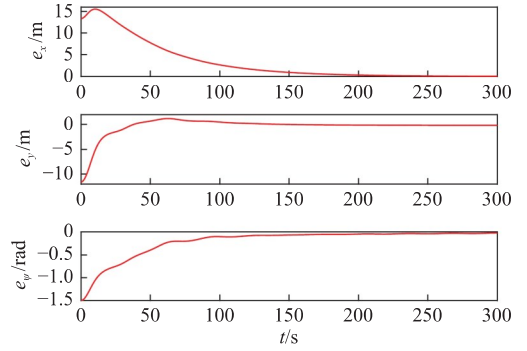


Fig. 4 Posture errors with scale factor

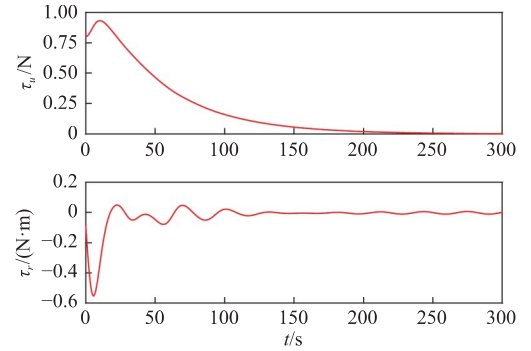


Fig. 5 Control input

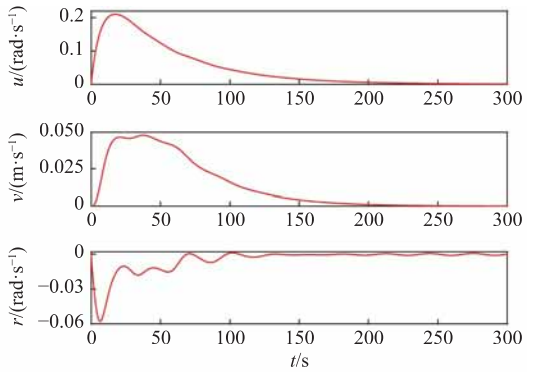


Fig. 6 Surge/sway velocity and yaw angle rate

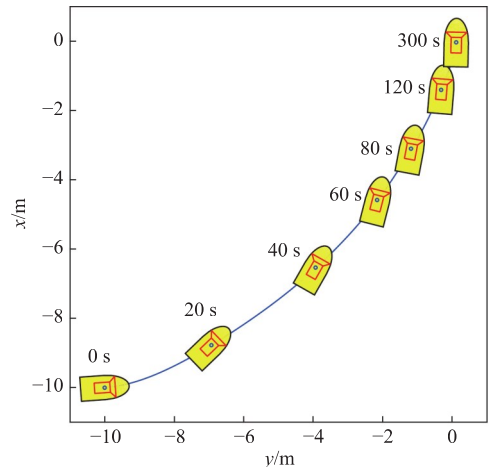


Fig. 7 The trajectory of an underactuated USV

the practical application of the visual servo method. Since the movement velocity of the USV is unknown, a continuous time-variant output feedback controller is designed to reduce the computational

complexity and ensure the real-time operation of the entire servo system.

The two control inputs are shown in Fig. 5, in which the continuous time invariant-control input  $\tau_u$  is used to stabilize the longitudinal position error, and the continuous time-variant control input  $\tau_r$  generates a continuous excitation signal according to the longitudinal position error, which changes the yaw angle of the USV and reduces the lateral position error of the underactuated USV. In addition,  $\tau_r$  is used to adjust the yaw angle of the USV to make it converge to the desired value. Although the USV monocular visual stabilization control system has unknown image depth, movement velocity, and model parameters, the posture errors of the underactuated USV are still asymptotically convergent to the origin under the effect of control inputs, and the movement velocity is asymptotically convergent to 0, as shown in Fig. 6, which is consistent with the aforementioned stability analysis. The underactuated USV continuously adjusts its position and posture according to the measurement information of the onboard monocular camera and gradually reaches the desired posture. The overall control effect is shown in Fig. 7.

To sum up, the designed continuous time-variant output feedback controller can overcome the non-integrable second-order nonholonomic constraints under the premise that the image depth, movement velocity, and model parameters are unknown by only using the image information of the onboard monocular camera, and it can achieve the asymptotic stability of the monocular visual servo stabilization control system of the underactuated USV.

## 4 Conclusions

To solve the stabilization control problem of the underactuated USV in GPS-denied environments, a monocular visual servo method with continuous time-variant output feedback is proposed in this paper, which realizes the asymptotic stability of the closed-loop control system when the image depth, movement velocity, and model parameters are unknown. Specifically, the homography decomposition technique is used to recover the posture errors with a scale factor directly from the current and desired images, which avoids the tedious processing of calibrating the external parameters of the camera and the target model information in advance. In order to overcome the underactuated property of USVs, the lateral position error and yaw angle error

are coupled, and a continuous time-variant output feedback controller is designed by incorporating a time-variant periodic function. It is worth noting that the system does not make additional estimations or observations of the unknown image depth and movement velocity, which greatly reduces the computational complexity of the controller. The Lyapunov theory and Barbalat lemma are used to rigorously prove the stability of the closed-loop control system. Simulation results have verified the effectiveness of the proposed visual servo stabilization control method. Future research work will consider the external disturbances of the underactuated UAV to improve the robustness of the monocular visual servo controller.

## References

- [1] LIU X, YE X M, WANG Q B, et al. Review on the research of local path planning algorithms for unmanned surface vehicles [J]. Chinese Journal of Ship Research, 2021, 16 (Supp 1): 1–10. (in Chinese)
- [2] OUYANG Z L, WANG H D, HUANG Y, et al. Path planning technologies for USV formation based on improved RRT [J]. Chinese Journal of Ship Research, 2020, 15(3): 18–24. (in Chinese)
- [3] YU Y L, SU R B, FENG X, et al. Tracking control of backstepping adaptive path of unmanned surface vessels based on surge-varying LOS [J]. Chinese Journal of Ship Research, 2019, 14(3): 163–171. (in Chinese)
- [4] WANG N, AHN C K. Hyperbolic-tangent LOS guidance-based finite-time path following of underactuated marine vehicles [J]. IEEE Transactions on Industrial Electronics, 2020, 67(10): 8566–8575.
- [5] BROCKETT R W. Asymptotic stability and feedback stabilization [C]//Differential Geometric Control Theory. Boston, MA: Birkhäuser Boston, 1983: 181–191.
- [6] GHOMMAM J, MNIF F, DERBEL N. Global stabilization and tracking control of underactuated surface vessels [J]. IET Control Theory & Applications, 2010, 4 (1): 71–88.
- [7] REYHANOGLU M. Exponential stabilization of an underactuated autonomous surface vessel [J]. Automatica, 1997, 33(12): 2249–2254.
- [8] GHOMMAM J, MNIF F, BENALI A, et al. Asymptotic backstepping stabilization of an underactuated surface vessel [J]. IEEE Transactions on Control Systems Technology, 2006, 14(6): 1150–1157.
- [9] PETTERSEN K Y, FOSSEN T I. Underactuated dynamic positioning of a ship-experimental results [J]. IEEE Transactions on Control Systems Technology, 2000, 8(5): 856–863.
- [10] MAZENC F, PETTERSEN K, NIJMEIJER H. Global uniform asymptotic stabilization of an underactuated surface vessel [J]. IEEE Transactions on Automatic Control, 2002, 47(10): 1759–1762.

- [11] DONG W J, GUO Y. Global time-varying stabilization of underactuated surface vessel [J]. *IEEE Transactions on Automatic Control*, 2005, 50(6): 859–864.
- [12] DONG Z P, WAN L, LI Y M, et al. Block backstepping stabilization control of underactuated USV in polar coordinate system [J]. *Journal of Traffic and Transportation Engineering*, 2015, 15(4): 61–68. (in Chinese)
- [13] DING W D, XU D, LIU X L, et al. Review on visual odometry for mobile robots [J]. *Acta Automatica Sinica*, 2018, 44(3): 385–400. (in Chinese)
- [14] HE H K, WANG N. Monocular visual servo of unmanned surface vehicles with view-field constraints [C]//2012 33rd Chinese Control and Decision Conference (CCDC). Kunming, China: IEEE, 2012: 973–978.
- [15] MARTINS A, ALMEIDA J M, FERREIRA H, et al. Autonomous surface vehicle docking manoeuvre with visual information [C]//Proceedings 2007 IEEE International Conference on Robotics and Automation. Rome, Italy: IEEE, 2007: 4994–4999.
- [16] DUNBABIN M, LANG B, WOOD B. Vision-based docking using an autonomous surface vehicle [C]//2008 IEEE International Conference on Robotics and Automation. Pasadena, CA, USA: IEEE, 2008: 26–32.
- [17] KIM Y H, LEE S W, YANG H S, et al. Toward autonomous robotic containment booms: Visual servoing for robust inter-vehicle docking of surface vehicles [J]. *Intelligent Service Robotics*, 2012, 5(1): 1–18.
- [18] XU H B, LIU C, TIAN J D, et al. Autonomous docking system for USV based on vision and position system [J]. *Computer Engineering and Design*, 2021, 42(9): 2606–2613. (in Chinese)
- [19] ZHANG S J, WANG J H, ZHENG X, et al. Autonomous berthing method of underactuated unmanned surface vehicle based on visual servo [J]. *Ship Engineering*, 2020, 42(7): 144–151. (in Chinese)
- [20] WANG N, HE H K. Adaptive homography-based visual servo for micro unmanned surface vehicles [J]. *The International Journal of Advanced Manufacturing Technology*, 2019, 105(12): 4875–4882.
- [21] WANG N, HE H K. Extreme learning-based monocular visual servo of an unmanned surface vessel [J]. *IEEE Transactions on Industrial Informatics*, 2021, 17(8): 5152–5163.
- [22] WANG N, HE H K. Dynamics-level finite-time fuzzy monocular visual servo of an unmanned surface vehicle [J]. *IEEE Transactions on Industrial Electronics*, 2020, 67(11): 9648–9658.
- [23] ZOU L M, HU X K, WU J L. The properties and discrimination of the positive definite matrices [J]. *Acta Scientiarum Naturalium Universitatis Sunyatseni*, 2009, 48(5): 16–23. (in Chinese)
- [24] HURWITZ A. Über algebraische gebilde mit eindeutigen transformationen in sich [J]. *Mathematische Annalen*, 1892, 41(3): 403–442.
- [25] TAO G. A simple alternative to the Barbalat lemma [J]. *IEEE Transactions on Automatic Control*, 1997, 42(5): 698.
- [26] MIN Y Y, LIU Y G. Barbalat lemma and its application in analysis of system stability [J]. *Journal of Shandong University (Engineering Science)*, 2007, 37(1): 51–55, 114. (in Chinese)
- [27] LOWE D G. Object recognition from local scale-invariant features [C]//Proceedings of the Seventh IEEE International Conference on Computer Vision. Kerkyra, Greece: IEEE, 1999, 2: 1150–1157.
- [28] ZHANG Z Y. Flexible camera calibration by viewing a plane from unknown orientations [C]//Proceedings of the Seventh IEEE International Conference on Computer Vision. Kerkyra, Greece: IEEE, 1999, 1: 666–673.
- [29] FANG Y C, DIXON W E, DAWSON D M, et al. Homography-based visual servo regulation of mobile robots [J]. *IEEE Transactions on Systems, Man, and Cybernetics, Part B (Cybernetics)*, 2005, 35(5): 1041–1050.
- [30] FAUGERAS O D, LUSTMAN F. Motion and structure from motion in a piecewise planar environment [J]. *International Journal of Pattern Recognition and Artificial Intelligence*, 1988, 2(3): 485–508.
- [31] DO K D, PAN J. Global robust adaptive path following of underactuated ships [J]. *Automatica*, 2006, 42(10): 1713–1722.
- [32] DAI S L, HE S D, LIN H, et al. Platoon formation control with prescribed performance guarantees for USVs [J]. *IEEE Transactions on Industrial Electronics*, 2018, 65(5): 4237–4246.
- [33] GHOMMAM J, MNIF F, BENALI A, et al. Observer design for Euler Lagrange systems: application to path following control of an underactuated surface vessel [C]//2007 IEEE/RSJ International Conference on Intelligent Robots and Systems. San Diego, CA, USA: IEEE, 2007: 2883–2888.

# 欠驱动无人船单目视觉伺服镇定控制

何红坤<sup>1</sup>,王宁<sup>\*2</sup>

1 大连海事大学 船舶电气工程学院,辽宁 大连 116026

2 大连海事大学 轮机工程学院,辽宁 大连 116026

**摘要:** [目的] 针对全球定位系统拒止环境下的欠驱动无人船(USV)精准位姿镇定问题,提出一种基于单应性的欠驱动无人船单目视觉伺服镇定控制方法。[方法] 借助单应性分解技术,直接从当前图像和期望图像中重构出具有未知尺度因子的位姿误差,可完全摆脱相机外部参数标定和目标物先验信息;针对欠驱动约束,在连续时变输出反馈控制器中引入基于持续激励艏摇角的周期函数,使得欠驱动无人船能够在图像深度、运动速度、模型参数均未知的情况下实现镇定控制。[结果] 在李雅普诺夫理论框架下,采用芭芭拉引理严格证明了欠驱动无人船视觉伺服闭环控制系统的渐近稳定性。[结论] 仅采用船载单目相机,所提出的视觉伺服策略能够确保欠驱动无人船实现精准位姿镇定,为海上接驳对接、靠离泊、动力定位等实际需求提供重要技术支撑。

**关键词:** 欠驱动无人船; 单目视觉伺服; 镇定控制; 连续时变输出反馈